



Stockholm
University

Bachelor Thesis

Degree Project in
Marine Geology 15 hp

Methane hydrates: Investigating the influence of sediment type on modeled methane escape in the high latitude Northern Hemisphere

Rafael Barros Parigi



Stockholm 2021

Department of Geological Sciences
Stockholm University
SE-106 91 Stockholm

ABSTRACT

Methane hydrates have drawn the attention of climate scientists in the past decades due to the potency of methane as a greenhouse gas and the widespread occurrence of hydrates both in terrestrial and marine environments, which, if destabilised, could enhance global warming. This study aims to investigate how much impact sediment type has on modeled methane escape at the feather edge of stability for methane hydrates in the high latitude Northern Hemisphere (45° to 75° N). This area is characterised by cool bottom-water temperatures leading to a shallow gas hydrate stability zone (GHSZ), and has been disproportionately influenced by contemporary seawater warming. Calculations were performed to establish the depths of the upper and lower boundaries of the feather edge of the GHSZ. These limits were used to estimate seafloor areas covered by three select sediment types that have different petrophysical properties - hemipelagic clay, calcareous ooze and siliceous ooze. Modeling of methane flux for 300 years following a 3°C warming during the first 100 years was performed using TOUGH + HYDRATE for each of the three sediment types. The sediments behaved significantly differently, with siliceous ooze releasing the most methane gas, and calcareous ooze releasing the least. Estimates of total methane gas release were also performed on the areas covered by the three sediments between latitudes 45° to 75° N, and showed that, over the course of 300 years, up to 5 times the current methane concentration in the atmosphere could become susceptible to leaving methane hydrate reservoirs.

Table of Contents

1. INTRODUCTION	3
1.1 Estimates of future release – numerical models.....	6
1.2 Petrophysical properties of sediments.....	7
2. METHODS	8
2.1 Calculation of the depth of the GHSZ.....	8
2.2 Extraction of the sediment lithologies above 45°N	10
2.3 Petrophysical models for key sediment types:.....	12
2.4 Modeling set-up using T+H:.....	15
3. RESULTS AND DISCUSSION	15
4. CONCLUSION	19
5. ACKNOWLEDGEMENTS	20
6. REFERENCES	21
7. APPENDIX 1.....	24
8. APPENDIX 2.....	25

1. INTRODUCTION

Methane is an important part of the carbon cycle and it has an atmospheric concentration of 1884 ppb (NOAA, 2020). Whilst carbon dioxide concentration is higher at 411.53 ppm (NOAA, 2020), methane is around 25 times more potent as a greenhouse gas than carbon dioxide (Hansen et al., 1988). In marine sediments methane is mainly produced through anaerobic decomposition of organic matter by microbes of the group archaea. Photolytic processes can break down methane after ten years in the atmosphere to carbon dioxide, whereas aerobic and anaerobic oxidation of methane represent the main sinks for methane in the oceans (Reeburgh, 2007).

Methane hydrates are a form of gas hydrate composed of methane molecules bound within a lattice of frozen water molecules. They have an average composition of $\text{CH}_4 \cdot (5.99 \pm 0.07)\text{H}_2\text{O}$ (Circone et al., 2005). Methane hydrates have drawn considerable attention from climate scientists due to the large volume believed to exist within marine sediments and also due to its potential as an energy resource, even though just a small percentage is accessible with current technologies.

One of the biggest issues surrounding gas hydrates is the great uncertainty in the estimates of the global reserves. Estimates of methane present in global hydrates vary substantially (Figure 1). Early estimates of hydrates were made before the actual recovery of gas hydrates from marine sediments, and assumed they were present everywhere where temperature and pressure conditions enabled their stability (Beaudoin et al., 2014). This would result in gas hydrates existing in sediments under around 93% of oceans on Earth (Milkov, 2004). Estimates were substantially reduced when probable occurrences of gas hydrate were limited to areas where a large enough supply of organic matter was present to fuel anaerobic decomposition.

Gas hydrates are stable within specific pressure and temperature conditions, with minor influences exerted by pore water chemistry, guest molecule composition, and guest molecule abundance (Thakore and Holder, 1987). Broadly speaking, high pressure and low temperatures are required which, due to Earth's geothermal gradient, can only be achieved within a finite area below the seafloor where high pressures are accompanied by relatively cool in-situ temperatures (Figure 2). This window of stability is called the gas hydrate stability zone (GHSZ), which is usually met at continental margins and is shaped as a "lens" that starts at a shallow depth, and gets thicker with depth as pressure increases (Stranne et al., 2016). Since bottom-water temperatures and geothermal gradients vary across the oceans, the depth and thickness of the GHSZ is quite variable (Dickens, 2001).

On continents, the permafrost regions around the Arctic have low-enough temperatures for the presence of the GHSZ, from around 200 to 300 meters below the land surface to 500 meters or more below the base of permafrost. In the oceans, the top of the GHSZ generally occurs at water depths of 300 to 500 meters or more, with the top of the GHSZ within the water column and the bottom below the sea floor (Beaudoin et al., 2014).

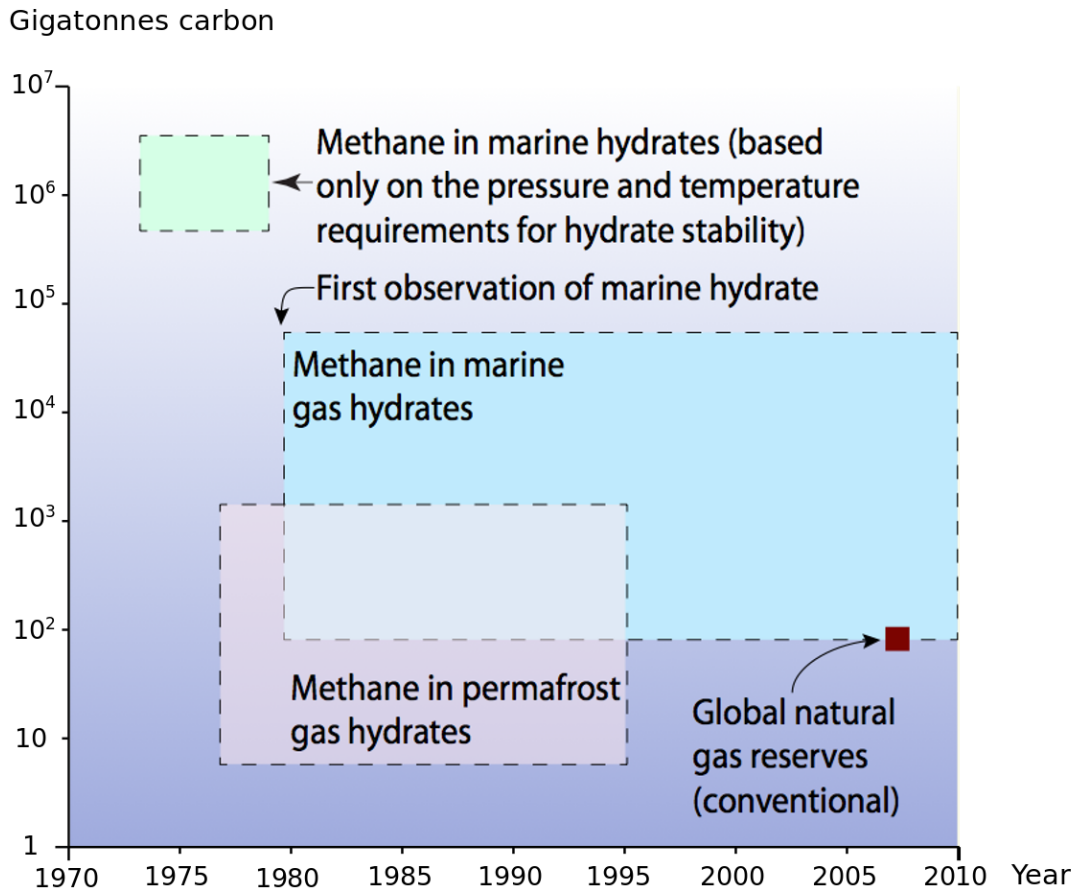


Figure 1. Estimates of methane stored in hydrates worldwide. The green zone shows very high early estimates before hydrates were first recovered from the oceans. The estimates were later reduced, but still highly variable due to the uncertainty in the amount/distribution of organic carbon. Even today, marine hydrate deposits are believed to store one to two orders of magnitude more methane than what is present in natural gas reserves across the planet. Figure from Beaudoin et al. (2014).

Gas hydrates do not exist everywhere in the GHSZ. The gas hydrate occurrence zone (GHOZ) is the region where gas hydrates actually exist. Most of the organic material resulting from primary productivity in the oceans, needed for the production of methane, is currently being deposited in shallow waters near continental margins. During glacial periods, when global sea-level was up to 140m lower than today, organic matter deposition occurred farther from the current continental margins, on today's continental slopes (Jasper and Gagosian, 1990). The lack of organic carbon deposition in deep ocean basins is why they are relatively free of methane hydrates, and why most contemporary work on marine methane hydrates occurs in continental shelf and slope settings (Ruppel, 2011).

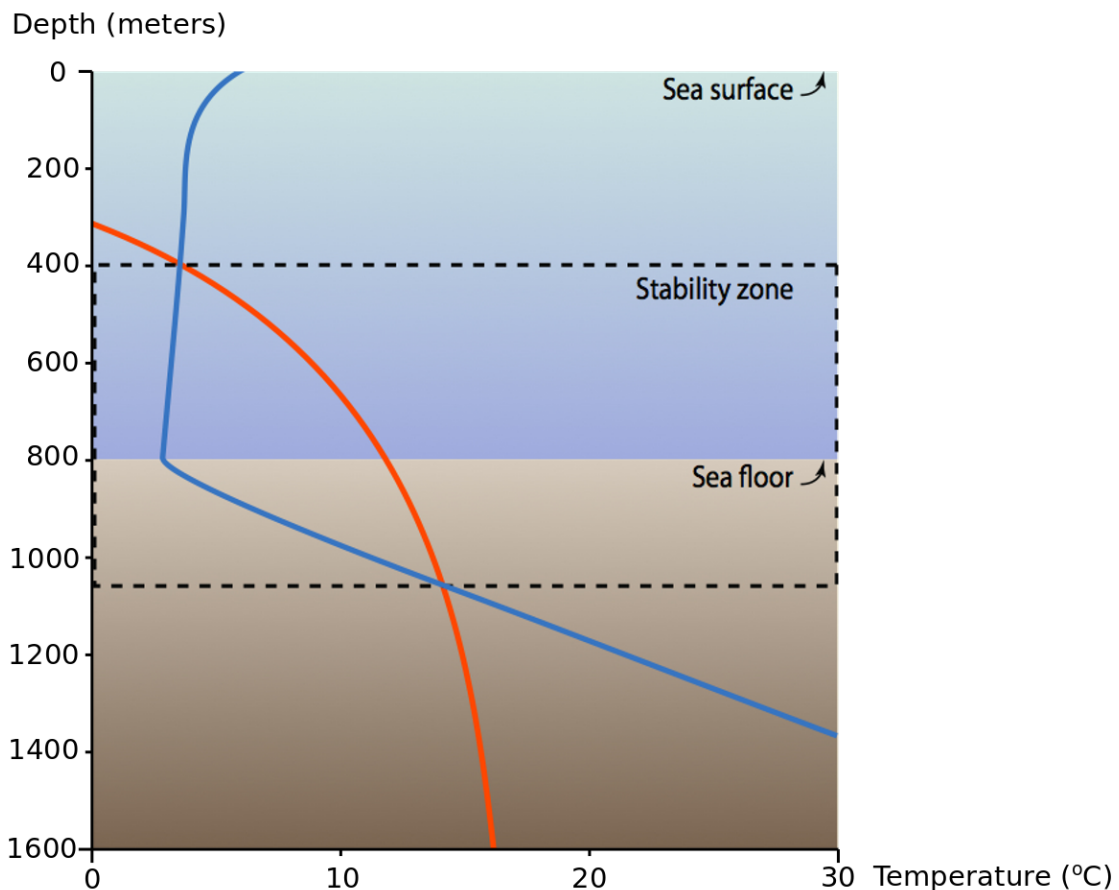


Figure 2. Idealised stability conditions for gas hydrates in a marine setting. The stability zone exists where the temperature (blue line) is less than the maximum stability temperature for a gas hydrate (orange line). The salt in seawater is a gas hydrate inhibitor, which moves the stability (orange) line to lower temperatures, thus reducing the stability window. Figure from Beaudoin et al. (2014).

Continued warming of ocean waters is predicted to cause a displacement of the gas hydrate stability zone to lower depths. This may potentially release large amounts of methane to the oceans and atmosphere. To assess the implications of potential destabilisation of methane hydrates in the oceans, it is essential to understand not only where the reserves of hydrates are found, but also the potential amount of methane gas that could escape from the sediments. For instance, from the middle and lower continental slope and deeper (usually greater than 500 meters water depth), where large deposits of methane hydrates exist (about 95% of all gas hydrates), it is not thought that these areas will be greatly affected by increased bottom-water temperatures in the next centuries (Reagan and Moridis, 2008). Despite possible bottom-water warming, these sediments will remain within the GHSZ due to the high pressure exerted by the water column. Heating would also need to take place for thousands of years to dissociate hydrates at the bottom of the GHSZ found along the middle and lower continental slopes (Xu et al., 2001) as heat can only penetrate the sea floor slowly via conduction.

However, the shallower waters of the upper continental slope (about 300-500 meters water depth) are much more susceptible to destabilisation as they are sensitive to

even moderate warming. In theory, the whole gas hydrate reservoir in this zone could be transformed into water and methane, which could escape the sediment's methane biofilter and reach seawater (Beaudoin et al., 2014). While gas hydrates situated near the surface could break down immediately upon seafloor warming, at depth it could take several hundred years as heat slowly propagates deeper into the sediments (Reagan and Moridis, 2008). Ruppel et al. (2011) estimates that around 3.5 percent of all gas hydrates on Earth are found at the upper continental slope. The most susceptible region to destabilisation on the upper continental slope is named the 'feather edge of hydrate stability', i.e. the area where the top and the bottom of the "lens-shaped" GHSZ (Figure 3) intercepts the seafloor as a result of decreasing pressure/depth and increasing bottom water temperature (Ketzer et al, 2020).

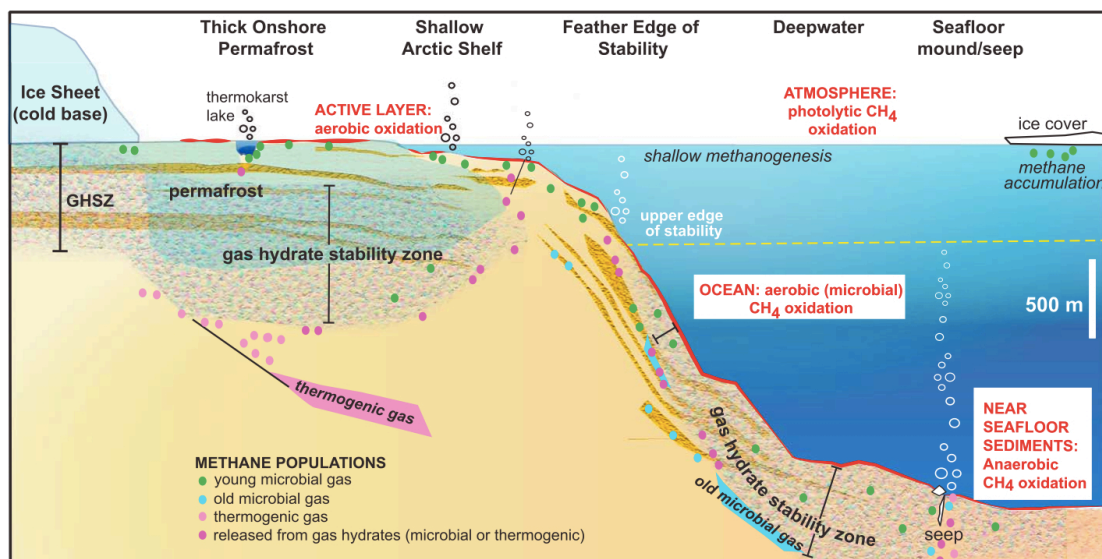


Figure 3. This schematic from Ruppel and Kessler (2017) shows methane hydrate dynamics and methane distributions in different settings. Gas hydrates on the feather edge (or upper edge) of stability on the upper continental slopes are particularly susceptible to dissociation.

1.1 Estimates of future release – numerical models

There are many complex factors that regulate the release of methane from seafloor sediments after its dissociation from hydrate. In order to estimate potential future methane release, numerical models have been developed which can address the intricacies of multiphase (mixed gas and liquid) flow through marine sediments. Through applying such models, Reagan and Moridis (2008) were able to show that substantial amounts of methane are trapped within sediments on a centennial timescale upon gas hydrate breakdown, implying that one cannot assume that all methane within dissociating hydrate reserves will escape from the seabed.

The TOUGH+HYDRATE (T+H) model (Moridis, 2014) is a computational model developed for simulating hydrate-bearing geologic media, and it has the capacity to do so at global scales. It can model the non-isothermal gas release, phase

behaviour, flow of fluids and heat in elaborate geologic systems. It solves the coupled equations of heat and mass balance and can describe hydrate phase changes, effects of inhibitors, hydrate formation and dissociation mechanisms.

For the accuracy of the simulations performed by T+H, it is important that the model takes into account not only the thermal changes (bottom water warming/geothermal gradients), but also the variations in sediment petrophysical properties that house the hydrates. Stranne et al. (2016) used a model setup for T+H where permeability, porosity, and thermal conductivity depend on depth, as the loss of porosity with greater depth leads to a non-linear decrease in permeability and a non-linear increase in thermal conductivity (Stranne and O'Regan, 2016).

1.2 Petrophysical properties of sediments

Petrophysical properties play an important role in determining not only the amount of methane hydrates that could be stored in sediments (via porosity and compressibility), but also how susceptible these sediments are to allowing the escape of methane gas (via permeability) and how fast they transmit heat to underlying strata (via thermal conductivity). The physical properties of sediments are largely determined by their composition. Dutkiewicz et al. (2016) divides seafloor sediments in 4 main classes (which are further subdivided into 13 lithologic classes): siliciclastic (comprising gravel, sand, silt, clay), volcanoclastic (ash and volcanic sand/gravel), transitional (fine grained calcareous sediment, siliceous mud), and biogenic (calcareous ooze, radiolarian ooze, diatom ooze, sponge spicules, mixed calcareous-siliceous ooze, shells and coral fragments). All these lithologies have different petrophysical properties, which will consequently impact how they can store and release methane hydrates.

Porosity (i.e. the percentage of void space) determines how much space is available for hydrates to form within sediments. Martin et al. (2015) consider porosity to be the most meaningful parameter when studying the seafloor, and having accurate measurements of porosity is fundamental for wide-scale modeling, as well as for determining sediment density, sound speed, thermal conductivity, electrical conductivity, and hydraulic conductivity. Permeability governs the rate of fluid flow through marine sediments. The burial depth and the sediment type are key components in determining sediment permeability. Porosity and sediment type affect the permeability of seafloor sediments, which can vary by seven orders of magnitude, from approximately 10^{-19} to 10^{-12} (Bryant and Rack, 1990). Thermal conductivity imposes a restriction on the rate of heat transfer through sediments.

Therefore, the purpose of this study is to investigate the influence that sediment type has on the magnitude and timing of modeled methane escape from the most vulnerable zones for marine methane hydrate dissociation.

2. METHODS

In this section, the depth interval for the feather edge of stability was estimated for the high latitude Northern Hemisphere. The corresponding sediment types were extracted for this depth range from the digital compilation of Dutkiewicz et al. (2016). Depth-dependent petrophysical properties, such as porosity, permeability, and thermal conductivity, were defined for these sediment types, which were used as parameters for the TOUGH + HYDRATE to model methane escape for 300 hundred years once the sediments are subjected to seafloor warming of 3°C.

2.1 Calculation of the depth of the GHSZ

The depths of the upper and lower boundaries of the GHSZ depend on temperature and pressure below the seafloor, and as a consequence it can be challenging to estimate these depths. This is because seafloor temperatures and seawater salinity can deviate from what is expected at different locations of the same latitude. Therefore despite complex temperature and salinity profiles, along with the presence of multiple gases across some areas of the seafloor, especially at locations of intense upward fluid advection (Ruppel et al., 2005), most areas with gas hydrates have in-situ salinity that follows that of seawater, in-situ pressures close to hydrostatic conditions, in-situ temperatures that resemble that of regional geothermal gradient, as well as methane being the most prevalent gas (Beaudoin et al., 2014). For this study, it was assumed that methane was the only gas present, whilst a representative temperature profile was estimated from the potential temperature by Schlitzer (2002) at site A24N, located approximately at latitude 60°N (Figure 4).

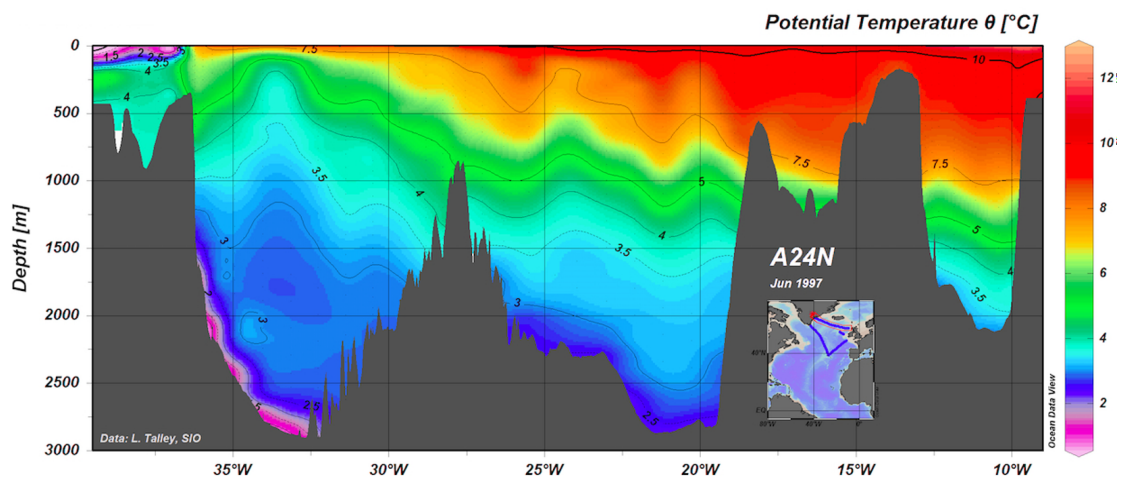


Figure 4. Potential temperature profile at location A24N (Schlitzer, 2002).

An empirical equation (Equation 1) was derived between temperature and depth by using the data extracted from A24N assuming a constant salinity of 35g/L (Figure 5).

$$D = -1576 \ln(T) + 3454.9 \quad (\text{eq 1})$$

Where,

D= Depth below sea surface (m)

T= Temperature (°C)

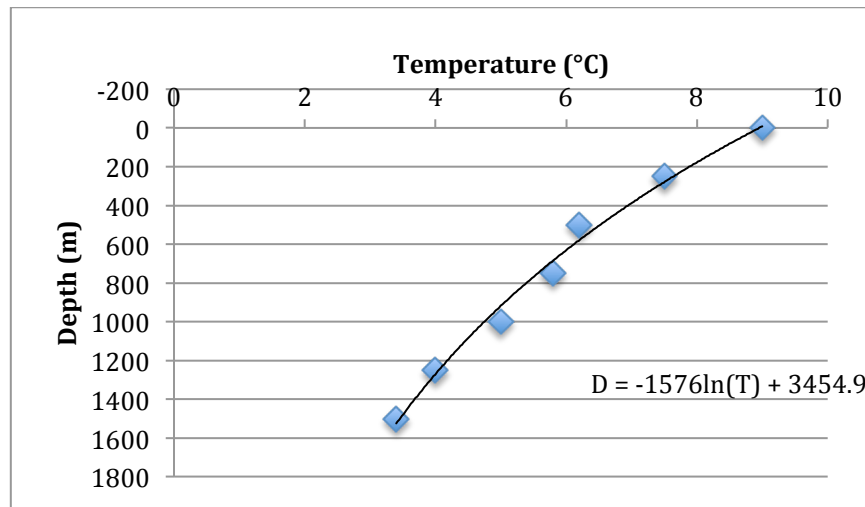


Figure 5. Estimated temperature versus depth (below the sea surface) for the A24N site of Schlitzer (2002), located in the North Atlantic.

In order to determine the areas within the feather edge of stability for methane hydrates, we have to know the depths in which they are stable. The dissociation pressure (P_{dis}^{SW}), i.e. the pressure where methane hydrates become unstable, was calculated using the formula by Tishchenko (2005) (Equation 2). This pressure was converted to a corresponding depth. However, Equation 2 does not provide the temperature at the dissociation depth. For this reason, it must be used in conjunction with equation 1 to generate an estimate of the depth of the upper boundary of the GHSZ in the high latitude Northern Hemisphere.

$$\ln(P_{dis}^{SW}/\text{MPa}) = -1.6444866 \times 10^3 - 0.1374178 \times T + 5.4979866 \times 10^4 / T + 2.64118188 \times 10^2 \ln(T) + S \times [1.1178266 \times 10^4 + 7.67420344 \times T - 4.515213 \times 10^{-3} \times T^2 - 2.04872879 \times 10^5 / T - 2.17246046 \times 10^3 \times \ln(T)] + S^2 \times [1.70484431 \times 10^2 + 0.118594073 \times T - 7.0581304 \times 10^5 \times T^2 - 3.09796169 \times 10^3 / T - 33.2031996 \times \ln(T)]. \quad (\text{eq. 2})$$

Where

P_{dis}^{SW} = dissociation pressure (MPa)

T= Temperature (°C)

S= Salinity (g/kg)

Calculating the correct upper boundary of dissociation pressure (or its respective dissociation depth) becomes an iterative exercise (Table 1). Upon choosing an initial estimate of 500m (T= 6.20°C; Equation 1) the dissociation depth was calculated as 554.7m (Equation 2). However, at the depth of 554.7m, the temperature is calculated by Equation 1 to be 6.30°C. These values form the inputs for the next iteration. Through each of these iterations, the dissociation depth calculated by Equation 2 and the depth corresponding to the temperature calculated by Equation 1 converge to a single value, equal to the upper boundary of dissociation pressure. After the third iteration (table 1) the dissociation pressure doesn't vary significantly, so this is the

value we assume for its upper boundary (560m depth when rounded to the nearest integer).

	Iteration 0	Iteration 1	Iteration 2	Iteration 3
Depth (m)	500	554.7	560.7	558.9
Temperature (°C)	6.20	6.30	6.27	6.28
Salinity (g/kg)	35.0	35.0	35.0	35.0
Dissociation pressure (MPa)/ Dissociation depth (m)	5.54/ 554.7	5.60/ 560.7	5.58/ 558.9	5.59/ 559.5

Table 1. Iterative method for calculating dissociation pressure/depth for methane hydrates. Based on equation by Tishchenko (2005).

Using Equation 2 and assuming a minimum possible temperature for seawater of 0°C, the lower boundary of dissociation pressure is at a depth of 293m.

As in the research by Stranne et al. (2016), this study does not consider seafloor depths below that of the calculated boundaries of the GHSZ, as even though gas is created at the base of the GHSZ, it cannot make its way up through the overlying hydrates. Our zone of interest for the rest of this study, i.e. the feather edge of methane hydrate stability, was estimated as 293m – 560m.

2.2 Extraction of the sediment lithologies above 45°N

The distribution of sediments in the oceans varies according to the source and transport pathways of sediment, which are largely controlled by climatic processes like weathering and diagenesis (Spinelli et al., 2004). For the purpose of this study, a map of the Northern Hemisphere, centered around the location A24N (Schlitzer, 2002) at 60°N with latitudes constrained between 45°N and 75°N (60°N +/- 15°), was developed using QGIS software (Figure 6). Two layers were used: a bathymetry layer (GEBCO, 2020) and seafloor sediment type layer (Dutkiewicz et al., 2016). A filter was applied on the bathymetry layer so that only depths between 293 and 560 meters deep were considered when displaying seafloor sediment types (Appendix 1). Sediment types followed Dutkiewicz et al. (2016) classification that has 4 main classes, which are further subdivided into 13 lithologic classes.

The vast majority of the sediments in the highest latitudes are composed of clay and siliceous mud. Further south, at the latitude of the British Isles, more sand and calcareous oozes are present. In order to encompass a good variety of sediments for this study, 3 sediment types were selected following the Dutkiewicz et al. (2016) classification, which represent some of the most frequently-found sediments in the study area. These included hemipelagic clay, which is classified as simply clay in Dutkiewicz et al. (2016), but we assume it to be hemipelagic clay as the locations in figure 6 are generally proximate to continental margins; siliceous ooze (siliceous mud in Dutkiewicz et al. (2016)), and calcareous ooze. The area covered by each of these three sediments between latitudes 45° and 75°, between longitudes -180° and 180°,

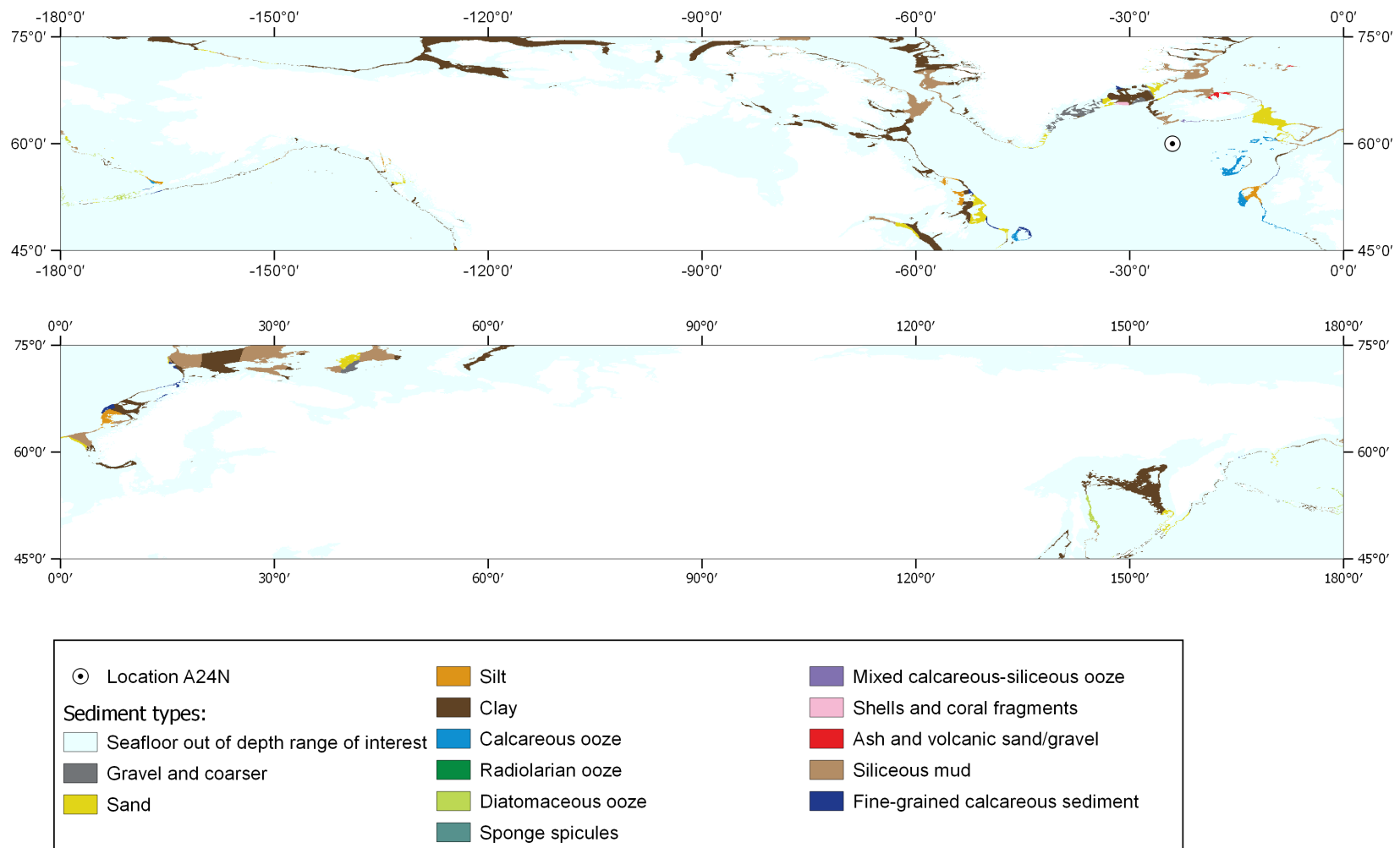


Figure 6. Seafloor sediment types at locations with seafloor depth between 293 and 560 meters deep. Built using seafloor sediment type layer by Dutkiewicz et al. (2016) and gridded bathymetry layer by GEBCO (2020) using QGIS (Coordinate Reference System: WGS 84).

between depths 293m and 560m from sea surface (table 2) was given by QGIS once the map was reprojected as a cylindrical equal area map.

Sediment type	Area (m ²)	Area (% of total seafloor area between latitudes 45° and 75°)	Area (% of feather edge area between latitudes 45° and 75°)
Hemipelagic clay	8.21 x 10 ¹¹	2.98%	52.81%
Calcareous ooze	5.57 x 10 ¹⁰	0.20%	3.58%
Siliceous ooze	3.44 x 10 ¹¹	1.25%	22.13%

Table 2. Sediment types selected for the analysis in this study and areas (in m² and as a percentage) occupied by them on Earth's feather edge of stability for latitudes between 45° and 75°.

2.3 Petrophysical models for key sediment types:

In order to model methane escape for the three selected sediment types, it was necessary to numerically determine their petrophysical properties. Porosity is a function of depth, whilst permeability is a function of porosity (Table 3). Thermal conductivity is a function of porosity and of the matrix's and fluid's individual thermal conductivities, and was calculated by applying the linear relationship between porosity and thermal conductivities of the matrix and fluid (equation 3).

	Porosity	Permeability
Calcareous ooze:	$0.72 - 0.987 \frac{D}{10^3} + 0.830 \left(\frac{D}{10^3}\right)^2$ (Hamilton, 1976)	$5.6 \times 10^{-21} e^{18\phi}$ (Spinelli et al., 2004)
Siliceous ooze (Diatomaceous ooze):	$0.861 - 0.549 \frac{D}{10^3} + 0.492 \left(\frac{D}{10^3}\right)^2$, (Hamilton, 1976)	$4.6 \times 10^{-23} e^{23\phi}$ (Spinelli et al., 2004)
Hemipelagic sediment:	$0.909 D^{-0.073}$ (Giambalvo, 2000)	$1.1 \times 10^{-18} e^{(2.2\phi)/(1-\phi)}$ (Spinelli et al., 2004)

Table 3. Equations that describe porosity and permeability with depth for calcareous ooze, siliceous (diatomaceous) ooze and hemipelagic sediment, where D is depth (m) and ϕ is porosity.

$$\lambda_B = \lambda_F \phi + \lambda_M (1 - \phi) \quad (\text{eq.3})$$

Where,

λ_B = Thermal conductivity of the bulk (W/mK)

λ_F = Thermal conductivity of the fluid (W/mK)

λ_M = Thermal conductivity of the matrix (W/mK)

\emptyset = Porosity

The fluid for the three sediments in this study was seawater ($\lambda_F = 0.6W/mK$ at $25^\circ C$ and salinity $35g/kg$). The matrix thermal conductivity was estimated based on the following assumptions:

- The calcareous ooze is composed of 50% saturated clay ($\lambda_{M1} = 2.47 W/mK$: O'Regan and Moran, 2010) and 50% calcium carbonate ($\lambda_{M2} = 3.59 W/mK$: Horai and Simmons, 1969).
- The siliceous ooze (diatomaceous ooze) is composed of 50% saturated clay ($\lambda_{M1} = 2.47 W/mK$) and 50% amorphous silica ($\lambda_{M2} = 1.2 \frac{W}{mK}$: Zhu et al., 2018).
- The hemipelagic sediment is composed of saturated clay only ($\lambda_{M1} = 2.47 W/mK$).

Porosity is modeled as being depth-dependent (Table 3), while permeability and thermal conductivity are both modeled as functions of porosity (Figures 7 – 9). Siliceous ooze is the most porous, most permeable, and has the lowest thermal conductivity. Calcareous ooze is the least porous, the least permeable below 370m deep, and has the highest thermal conductivity.

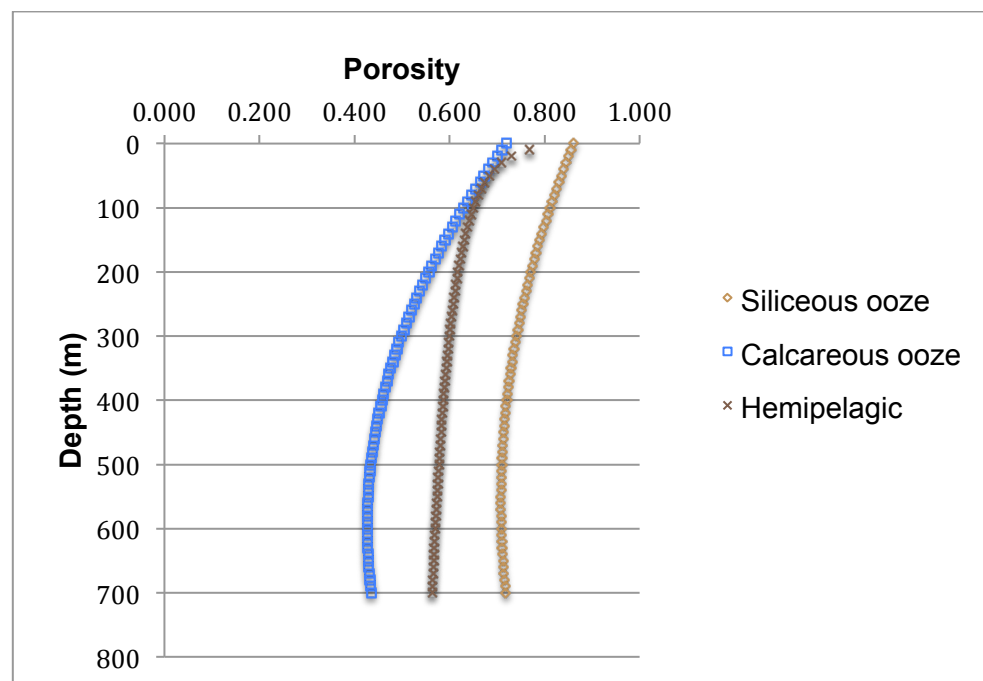


Figure 7. Porosity versus depth for siliceous, calcareous, and hemipelagic sediments. Calcareous and siliceous ooze porosity defined by Hamilton (1976), hemipelagic sediment is defined by Giambalvo (2000).

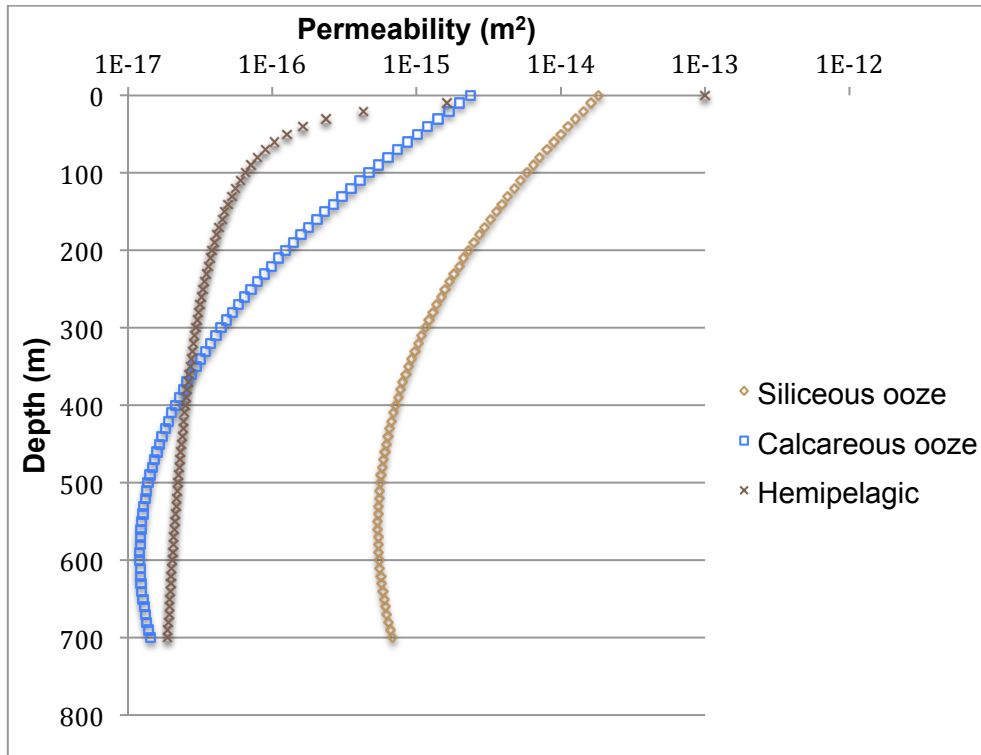


Figure 8. Permeability versus depth for siliceous, calcareous, and hemipelagic sediments. Permeability axis in logarithmic scale for better visualisation. Sediments have permeability defined by Spinelli et al. (2004).

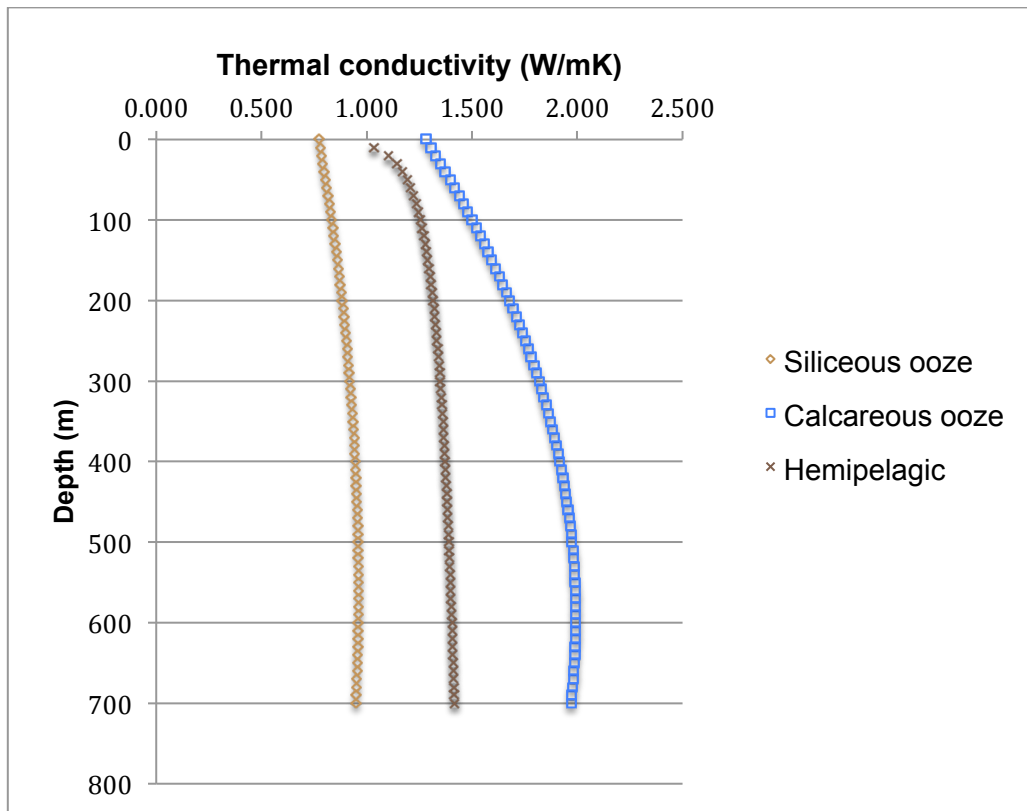


Figure 9. Thermal conductivity versus depth for siliceous, calcareous and hemipelagic sediments.

2.4 Modeling set-up using T+H:

T+H was run by Christian Stranne at the Department of Geological Sciences, Stockholm University. The modeling of the three cases was run over 300 years. This study assumes constant initial hydrate saturation (5%), bottom-water temperature (5°C) and heat flow (40 mW/m²), followed by a step change where seafloor temperature rises by 3°C over the first 100 years and then stabilises at this temperature.

Conductivity profiles for the different sediment types produced different temperature profiles, which resulted in different GHSZ depths for each type of sediment. For that reason, seafloor depth was adjusted in each case to ensure an initial GHSZ depth of 20 meters (seafloor depth - Hemipelagic case: 530 m; Calcareous case: 518 m; Siliceous case: 540 m). This allowed for more meaningful comparisons of modeling results.

3. RESULTS AND DISCUSSION

For each case, the total initial pool of methane is a mix of hydrate and dissolved gas (Figures 10, 11, 12). As the experiment starts with an increase in bottom-water temperature of 3°C, the methane pool holds fairly steady for a few years whilst heat slowly propagates further down through the sediments. Shortly, the methane hydrates start to break down and get converted into methane gas at an accelerating rate before this loss becomes linear. For siliceous ooze, this acceleration begins after approximately 26 years, after which time it starts to linearly lose approximately 1.0kg/m² of hydrate every year. For hemipelagic clay, the acceleration begins after approximately 20 years, after which it also starts to lose approximately 1.0kg/m² of hydrate every year. For calcareous ooze, it begins after approximately 11 years, after which it loses approximately 1.0kg/m² every year as well.

The dissolved pool remains fairly constant throughout the models. On the other hand, the gas pool increases in concentration (the source of the gas being the hydrate pool) as the rate of gas production is higher than the rate of gas escape from the sediments; it reaches its maximum concentration at the time when all hydrate is depleted from the models – this happens after 105 years for siliceous ooze, after 93 years for hemipelagic clay, and after only 74 years for calcareous ooze. From that point, the rate of gas escape is higher than the rate of gas production (which is zero) as there are no more hydrates to feed the system, hence the cumulative gas flux keeps increasing even after all the hydrates are consumed and long after bottom-water temperature stops increasing.

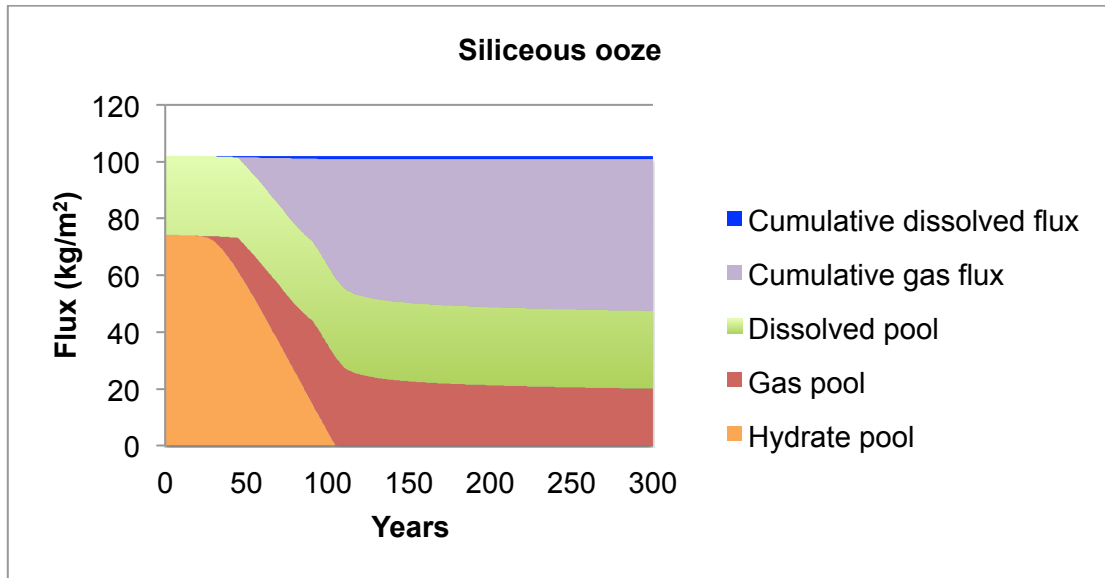


Figure 10. Results for simulation using T+H in siliceous ooze. For this model, bottom water temperature was warmed by 3°C in the first 100 years, and stabilized after that.

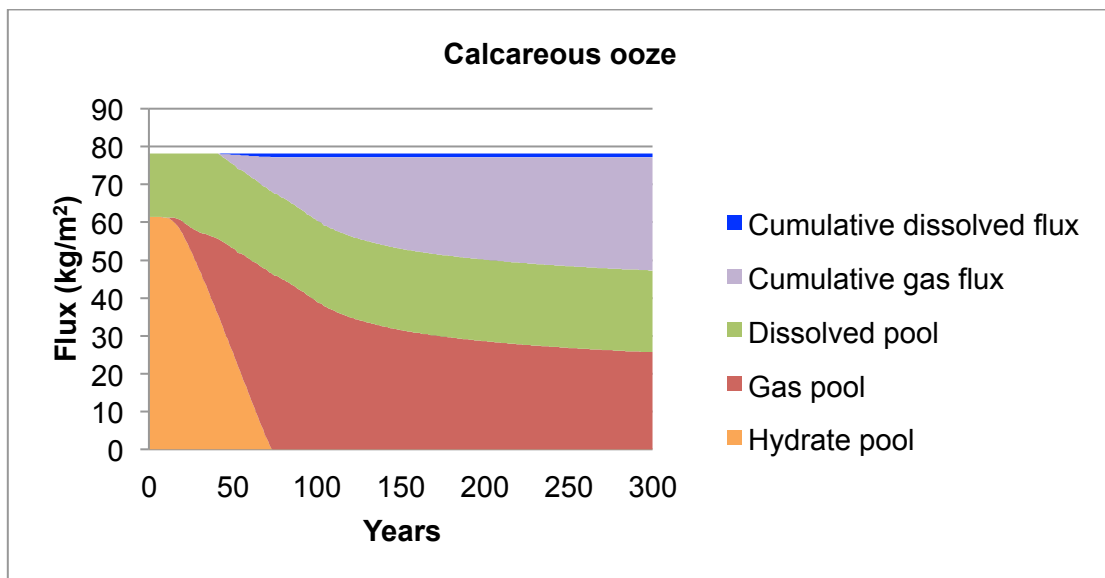


Figure 11. Results for simulation using T+H in calcareous ooze. For this model, bottom water temperature was warmed by 3°C in the first 100 years, and stabilized after that.

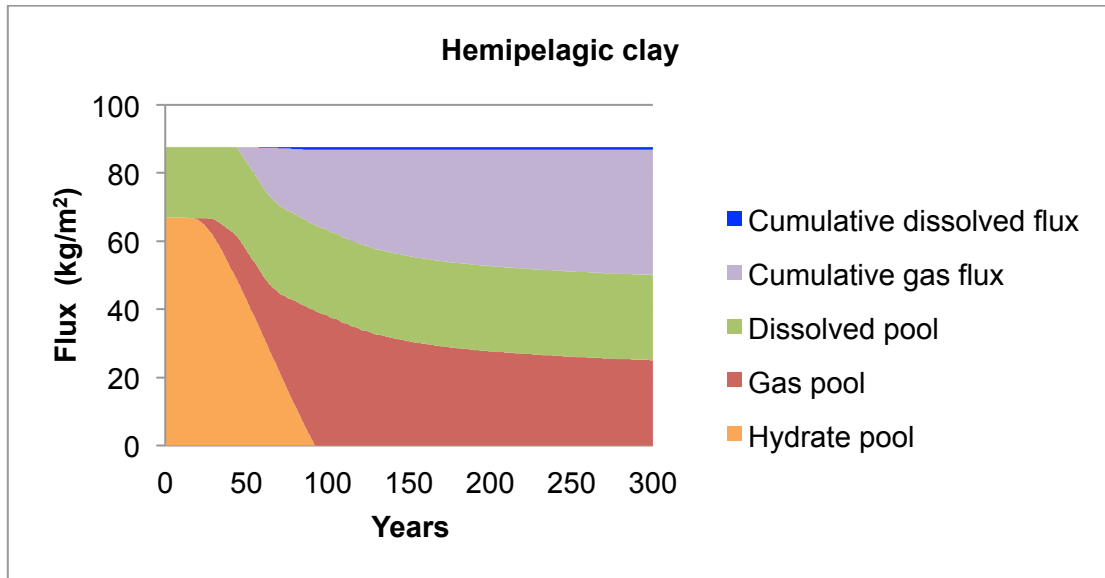


Figure 12. Results for simulation using T+H in hemipelagic sediment. For this model, bottom water temperature was warmed by 3°C in the first 100 years, and stabilized after that.

Siliceous ooze retains hydrate in its pore space for about 31 years longer than the calcareous ooze, with the hemipelagic sediment falling in between (Figure 13). This agrees with siliceous ooze having the highest porosity (Figure 7), thus being able to store more hydrates for longer, and calcareous ooze having lowest porosity out of the three sediments, at least in these relatively shallow (GHSZ of only 20 meters) experiments where fracturing doesn't occur.

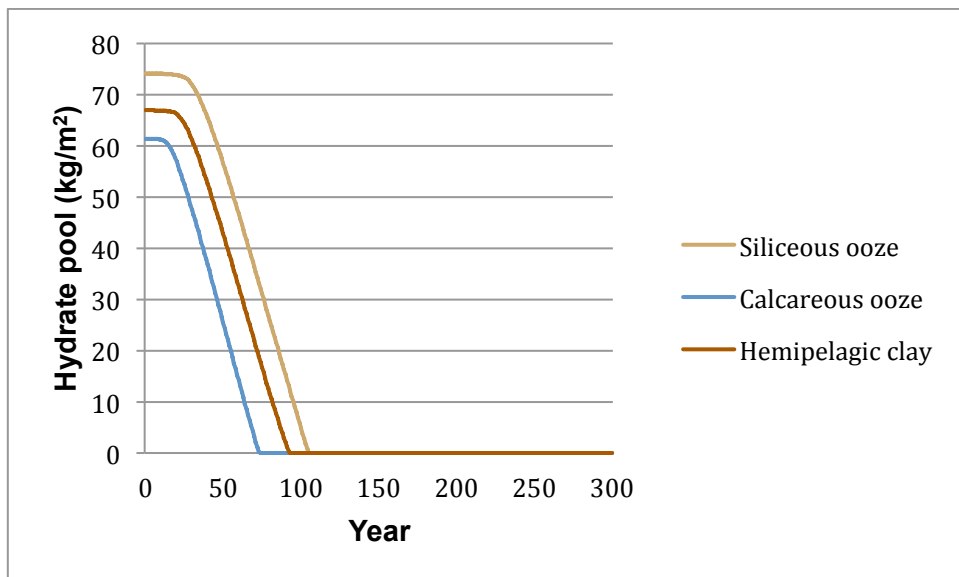


Figure 13. Evolution of methane hydrates over time for T+H simulation.

Despite holding hydrates for longer, siliceous ooze also ends up with the highest cumulative gas flux (53.41kg/m²) after 300 years (Figure 14), due to having the combination of highest porosity and permeability out of the three sediment types. On

the other hand, calcareous ooze, which has the lowest porosity and second lowest permeability ends up with lowest cumulative gas flux (29.93kg/m²).

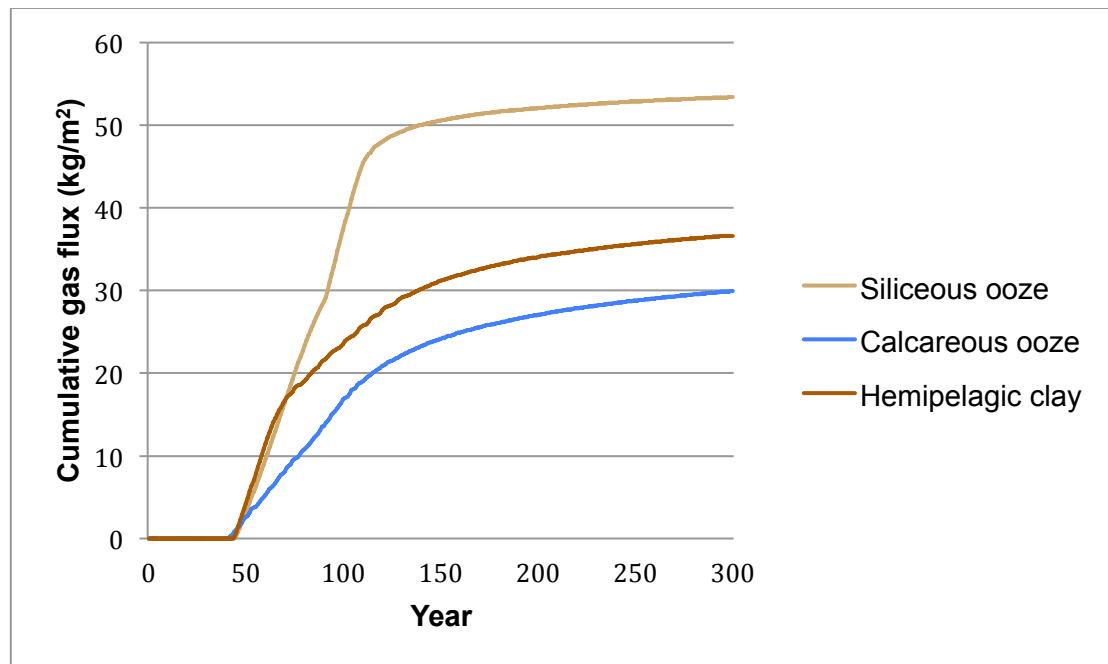


Figure 14. Cumulative methane gas release over time for T+H simulation.

Porosity seems to control how long sediments can hold methane hydrates, whereas a combination of high porosity and high permeability appears to lead to high cumulative gas flux. There's a significant difference in gas flux between the sediments, particularly between siliceous ooze and calcareous ooze. Further investigations are necessary to decipher the potential influences exerted by difference in geothermal gradients and dynamic processes such as hydro-fracturing.

Siliceous ooze appears to be the most vulnerable to methane escape out of the 3 sediment types considered in this study. When analysing the sediment distribution map (Figure 6), we can conclude that vast areas of the Arctic and North Atlantic – including the east coast of Canada, the seafloor surrounding Greenland and north of Scandinavia - are covered by siliceous ooze at the depths critical for methane hydrate breakdown. Hemipelagic sediment occurs at similar locations as siliceous ooze and also covers extensive areas, thus also requiring significant attention. On the other hand, calcareous ooze is found at the feather edge of stability mainly to the east of Newfoundland (Canada), to the west of Ireland, and between the British Isles and Iceland, and demand the least attention in terms of methane escape.

Taking the cumulative gas flux per unit area (Figure 14, Appendix 2) and the area occupied by each of the three sediment types (Table 2), their total cumulative gas flux is estimated (Table 4). After 300 years, the three sediments combined will have potentially released a total of 5.02×10^{13} kg of methane. Taking into account the total mass of Earth's atmosphere at 5.15×10^{18} kg (Trenberth and Smith, 2005) and current methane concentration at 1884 ppb (NOAA, 2020), we can infer that the total current mass of methane in Earth's atmosphere is 9.70×10^{12} kg. We can conclude that, considering the warming conditions used in our models, the methane escape

from our three sediments in our limited area of study alone would represent an addition of approximately 5 times the methane that is currently present in our atmosphere over the next 300 years.

Cumulative mass of methane (kg) for latitudes 45° - 75° and longitude -180° - 180°						
Sediment type	After 50 years	After 100 years	After 150 years	After 200 years	After 250 years	After 300 years
Hemipelagic clay	3.48×10^{12}	1.93×10^{13}	2.56×10^{13}	2.80×10^{13}	2.93×10^{13}	3.01×10^{13}
Calcareous ooze	1.43×10^{11}	9.39×10^{11}	1.35×10^{12}	1.51×10^{12}	1.60×10^{12}	1.67×10^{12}
Siliceous ooze	1.10×10^{12}	1.29×10^{13}	1.74×10^{13}	1.79×10^{13}	1.82×10^{13}	1.84×10^{13}

Table 4. Estimated methane release after 50, 100, 150, 200, 250 and 300 years from siliceous, calcareous and hemipelagic sediments at latitudes between 45° and 75°.

Finally, it's critical that the limitations of this study are acknowledged. The porosity and permeability relationships (Table 3) used for modeling the sediments are, according to Spinelli et al. (2004), empirical equations that provide best fits to the data at the conditions considered in those studies, but may not be a best fit for all the sediment data considered here. It was also assumed that the surface sediment composition of the seafloor defined by Dutkiewicz et al. (2016) remained constant through the upper 20m below the seafloor. Sediment cores obtained from across the Laptev Sea continental slope by Nürnberg et al. (1995) present only minor lithological changes throughout, which might not necessarily be true for other slope settings.

Moreover, at the current warming rate, the IPCC (2019) forecasts an increase in global mean sea level temperature between 1.64°C and 3.51°C, with a mean of 2.58°C, by the end of the century (2081 – 2100). Here it was assumed that seafloor temperatures would increase by 3°C for the hydrate modeling. The justification for assuming a greater increase in seafloor temperature is that this warming will be driven by the surface air temperature, which for the latitudes of the Arctic/North Atlantic, has increased at more than twice the global mean over the last two decades (IPCC, 2019). However, even small differences in this estimate could lead to significant differences in the amounts of methane gas released.

4. CONCLUSION

On continental slopes of the high Northern latitudes, where the feather edge of stability is at a shallower depth compared to most places on Earth due to lower temperatures, the dissociation of hydrates has either already begun or could begin within the next century, and will successively progress to lower latitudes (Biastoch et al., 2011). As a poorly-constrained source of greenhouse gas, and positive feedback

to global warming, it is paramount that we progress our understanding of methane hydrate behaviour in the context of climate change.

This study modeled the behaviour of three of the most common sediment types present in the high Northern Hemisphere where the feather edge of stability exists. There are significant differences in terms of methane retention/release between these sediment types, which are attributed to differences in petrophysical properties. Siliceous ooze, the most porous of the three sediments, can retain methane in its hydrate form for longer. It is, however, the most permeable of the sediments, and after 300 years its cumulative methane flux is nearly twice as high as calcareous ooze's after the same period of time.

Whilst most of the methane flux released from gas hydrate reservoirs is expected to be consumed in the sediment or water column prior to entering the atmosphere (Beaudoin et al, 2014), even a small increase in atmospheric methane concentration can have a significant impact on climate when we take into account methane's potency as a greenhouse gas. Moreover, under the modeled conditions, our estimates suggest that between latitudes 45° - 75°, up to 5 times more methane than currently exists at the Earth's atmosphere could become susceptible to leaving their original reservoirs in 300 years.

5. ACKNOWLEDGEMENTS

I would like to thank my supervisor Matt O'Regan for all the help and support for the past months. Without his expertise, his prompt replies to my emails, and his availability for our Zoom meetings, this work would not have been possible.

I would also like to thank Christian Stranne for his insights into this project and also for running the models on the sediments for this thesis.

Lastly, I want to thank my family and Angus Watt for all their support throughout not only this project, but through my whole life.

6. REFERENCES

Beaudoin, Y. C., Waite, W., Boswell, R. and Dallimore, S. R. (eds), 2014. *Frozen Heat: A UNEP Global Outlook on Methane Gas Hydrates*. Volume 1. United Nations Environment Programme, GRID-Arendal.

Biastoch, A., Treude, T., Rüpke, L.H., Riebesell, U., Roth, C., Burwicz, E.B., Park, W., Böning, C.W., Latif, M., Madec, G. and Wallmann, K. (2011). Evolution of Arctic Ocean temperatures and the fate of marine gas hydrates under global warming. *Geophys. Res. Lett.*, 38, doi:10.1029/2011GL047222.

Bryant, W. R. and Rack, F. R. 1990. Consolidation characteristics of Weddell Sea sediments. In *Proceedings of the Ocean Drilling Program, Scientific Results*, Vol. 113, eds. P. F. Barker and J. P. Kennet. College Station, TX: Ocean Drilling Program, pp. 211–223.

Circone, S., Kirby, S.H. and Stern, L.A. (2005). Direct measurement of methane hydrate composition along the hydrate equilibrium boundary. *J. Phys. Chem. B*, 109, 9468-9475.

Dickens, G. R. (2001), The potential volume of oceanic methane hydrates with variable external conditions, *Organic Geochemistry*, 32(10), 1179-1193.

Dutkiewicz A. et al. (2015), Census of seafloor sediments in the world's ocean, *Geology*, 43 (9): 795–798.

Dutkiewicz, A., S. O'Callaghan, and R. D. Mueller (2016), Controls on the distribution of deep-sea sediments, *Geochem. Geophys. Geosyst.*, 17, 3075– 3098, doi:10.1002/2016GC006428.

GEBCO Compilation Group (2020) GEBCO 2020 Grid (doi:10.5285/a29c5465-b138-234d-e053-6c86abc040b9)

Giambalvo, E. R., Fisher, A. T., Martin, J. T., Darty, L., and Lowell, R. 2000. Origin of elevated sediment permeability in a hydrothermal seepage zone, eastern flank of the Juan de Fuca Ridge, and implications for transport of fluid and heat. *J. Geophys. Res.* 105: 913–928.

Hamilton, E.L., 1976. Variations of Density and Porosity with depth in Deep-Sea sediments. *Journal of Sedimentary Petrology* 46, 280–300.

Hansen, J., Fung, A., Lacis, A., Rind, D. and Lebedeff, S. (1988). Global climate changes as forecast by Goddard Institute for Space Studies 3-D Model. *J. Geophys. Res.*, 93, 9341-9364.

Horai, K. and G. Simmons, Thermal conductivity of rock-forming minerals, *Earth Planet. Sci. Lett.*, 6, 359–368, 1969.

IPCC, 2019: Technical Summary [H.-O. Pörtner, D.C. Roberts, V. Masson-Delmotte, P. Zhai, E. Poloczanska, K. Mintenbeck, M. Tignor, A. Alegría, M. Nicolai, A. Okem, J. Petzold, B. Rama, N.M. Weyer (eds.)]. In: *IPCC Special Report on the Ocean and Cryosphere in a Changing Climate* [H.- O. Pörtner, D.C. Roberts, V. Masson-Delmotte, P. Zhai, M. Tignor, E. Poloczanska, K. Mintenbeck, A. Alegría, M. Nicolai, A. Okem, J. Petzold, B. Rama, N.M. Weyer (eds.)]. In press.

Jasper, J.P. and Gagosian, R.B. (1990). The sources and deposition of organic matter in the Late Quaternary Pigmy Basin, Gulf of Mexico. *Geochim. Cosmochim. Acta*, 54, 1117-1132.

Ketzer, M. et al. (2020), Gas hydrate dissociation linked to contemporary ocean warming in the southern hemisphere, *Nature Communications*, 11, 378, <https://doi.org/10.1038/s41467-020-17289>.

Martin, K. M., W. T. Wood, and J. J. Becker (2015), A global prediction of seafloor sediment porosity using machine learning, *Geophys. Res. Lett.*, 42, 10,640–10,646, doi:10.1002/2015GL065279.

Milkov, A. (2004). Global estimates of hydrate-bound gas in marine sediments: How much is really out there? *Earth-Sci. Rev.*, 66, 183-197.

Moridis, G (2014). User's Manual For The Hydrate V1.5 Option Of Tough+ V1.5: A Code For The Simulation Of System Behavior In Hydrate-Bearing Geologic Media, Earth Sciences Division, Lawrence Berkeley National Laboratory, Berkeley.

NOAA (National Oceanic and Atmospheric Administration), 'Carbon Cycle Greenhouse Gases', *Global Monitoring Laboratories*, 2021, <https://www.esrl.noaa.gov/gmd/ccgg/>, (accessed 22 January 2021).

Nürnberg, D., Fütterer, D. K., Niessen, F., Nørgaard-Pedersen, N., Schubert, C. J., Spielhagen, R. F., & Wahsner, M. (1995). The depositional environment of the Laptev Sea continental margin: preliminary results from the R/V Polarstern ARK IX-4 cruise. *Polar Research*, 14(1), 43-54. <https://doi.org/10.3402/polar.v14i1.6650>

O'Regan, M., and Moran, K., (2010). Deep-water methane hydrates in the Arctic Ocean: Re-assessing the significance of a shallow BSR on the Lomonosov Ridge. *Journal of Geophysical Research - Solid Earth*, 115. B05102.

Reagan, M.T. and Moridis, G.J. (2008). Dynamic response of oceanic hydrate deposits to ocean temperature change. *J. Geophys. Res.- Oceans*, 113. doi: 10.1029/2008jc004938.

Reeburgh, W.S. (2007). Oceanic methane biogeochemistry. *Chem. Rev.*, 107, 486-513.

Ruppel, C.D. (2011). Methane hydrates and contemporary climate change. *Nature Education Knowledge*, 2, 12

Ruppel, C. D., and J. D. Kessler (2017), The interaction of climate change and methane hydrates, *Rev. Geophys.*, 55, 126-168, doi:10.1002/2016RG000534.

Ruppel, C., G. R. Dickens, D. G. Castellini, W. Gilhooly, and D. Lizarralde (2005), Heat and salt inhibition of gas hydrate formation in the northern Gulf of Mexico, *Geophys. Res. Lett.*, 32, L04605, doi:10.1029/2004GL021909.

Ruppel, C., T. Collett, R. Boswell, T. Lorenson, B. Buczkowski, and Waite W. (2011), A new global gas hydrate drilling map based on reservoir type, *Fire in the Ice: Department of Energy, Office of Fossil Energy, National Energy Technology Laboratory, Methane Hydrate News Letter*, 11, 13-17.

Schlitzer, R. 2002. eWOCE - Electronic Atlas of WOCE Data. Alfred Wegener Institute for Polar and Marine Research, Bremerhaven, Germany. https://www.ewoce.org/gallery/Map_Atlantic.html (accessed 12 October 2020).

Spinelli, G., et al., 2004. Sediment permeability, distribution, and influence on fluxes in oceanic basement. *Hydrogeol. Ocean. Lithosphere*, 1, 151.

Stranne, C., and O'Regan, M. (2016). Conductive heat flow and nonlinear geothermal gradients in marine sediments—observations from Ocean Drilling Program boreholes. *Geo-Mar. Lett.* 36, 25–33.

Stranne, C., M. O'Regan, G. R. Dickens, P. Crill, C. Miller, P. Preto, and M. Jakobsson (2016), Dynamic simulations of potential methane release from East Siberian continental slope sediments, *Geochem. Geophys. Geosyst.*, 17, 872–886, doi:10.1002/2015GC006119.

Thakore, J.L. and Holder, G.D. (1987). Solid-vapor azeotropes in hydrate-forming systems. *Ind. Eng. Chem. Res.*, 26, 462 – 469.

Tishchenko P. et al. (2005), Calculation of the stability and solubility of methane hydrate in seawater, *Chemical Geology* 219: 37 – 52.

Trenberth, K. E, Smith, L (2005). The Mass of the Atmosphere: A Constraint on Global Analyses. *Journal Of Climate*, 18, 864 – 875.

Xu, W., R. P. Lowell, and E. T. Peltzer (2001), Effect of seafloor temperature and pressure variations on methane flux from a gas hydrate layer: Comparison between current and Late Paleocene climate conditions, *Journal of Geophysical Research*, 106(B11), 26413-26423.

Zhu, W., Zheng, G., Cao, S. *et al.* Thermal conductivity of amorphous SiO₂ thin film: A molecular dynamics study. *Sci Rep* 8, 10537 (2018). <https://doi.org/10.1038/s41598-018-28925-6>

7. APPENDIX 1

Two raster layers were used when building Figure 6 in QGIS: ETOPO1_Bed_c_geotiff@1, which is a bathymetry layer by GEBCO (2020) containing the bathymetric measurements of all of the Earth's oceans; and seabed_lithology_v1@1 by Dutkiewicz et al. (2016) containing sediment type coverage for Earth's oceans (with the exception of highest latitudes, i.e. 75° – 90° and -75° – -90°) which was divided in 13 sediment types.

In order to get only the sediment type coverage in the desired depths – between -293m and -560m below sea level – and to constrain it to the desired latitudes – between 45° and 75° – the raster calculator tool was used.

Each “n” out of the 13 sediment types in the interval between -293m and -560m depth was multiplied by its own value “n”, a syntax that assigns back to “n” whatever it was multiplied by.

The full calculation is as follows:

```
("ETOPO1_Bed_c_geotiff@1" < - 293 AND "ETOPO1_Bed_c_geotiff@1" > - 560
AND "seabed_lithology_v1@1" = 1) * 1
+ ("ETOPO1_Bed_c_geotiff@1" < - 293 AND "ETOPO1_Bed_c_geotiff@1" > - 560
AND "seabed_lithology_v1@1" = 2) * 2
+ ("ETOPO1_Bed_c_geotiff@1" < - 293 AND "ETOPO1_Bed_c_geotiff@1" > - 560
AND "seabed_lithology_v1@1" = 3) * 3
+ ("ETOPO1_Bed_c_geotiff@1" < - 293 AND "ETOPO1_Bed_c_geotiff@1" > - 560
AND "seabed_lithology_v1@1" = 4) * 4
+ ("ETOPO1_Bed_c_geotiff@1" < - 293 AND "ETOPO1_Bed_c_geotiff@1" > - 560
AND "seabed_lithology_v1@1" = 5) * 5
+ ("ETOPO1_Bed_c_geotiff@1" < - 293 AND "ETOPO1_Bed_c_geotiff@1" > - 560
AND "seabed_lithology_v1@1" = 6) * 6
+ ("ETOPO1_Bed_c_geotiff@1" < - 293 AND "ETOPO1_Bed_c_geotiff@1" > - 560
AND "seabed_lithology_v1@1" = 7) * 7
+ ("ETOPO1_Bed_c_geotiff@1" < - 293 AND "ETOPO1_Bed_c_geotiff@1" > - 560
AND "seabed_lithology_v1@1" = 8) * 8
+ ("ETOPO1_Bed_c_geotiff@1" < - 293 AND "ETOPO1_Bed_c_geotiff@1" > - 560
AND "seabed_lithology_v1@1" = 9) * 9
+ ("ETOPO1_Bed_c_geotiff@1" < - 293 AND "ETOPO1_Bed_c_geotiff@1" > - 560
AND "seabed_lithology_v1@1" = 10) * 10
+ ("ETOPO1_Bed_c_geotiff@1" < - 293 AND "ETOPO1_Bed_c_geotiff@1" > - 560
AND "seabed_lithology_v1@1" = 11) * 11
+ ("ETOPO1_Bed_c_geotiff@1" < - 293 AND "ETOPO1_Bed_c_geotiff@1" > - 560
AND "seabed_lithology_v1@1" = 12) * 12
+ ("ETOPO1_Bed_c_geotiff@1" < - 293 AND "ETOPO1_Bed_c_geotiff@1" > - 560
AND "seabed_lithology_v1@1" = 13) * 13
```

8. APPENDIX 2

Sediment type	Area (m ²)
Hemipelagic clay	8.21 x 10 ¹¹
Calcareous ooze	5.57 x 10 ¹⁰
Siliceous ooze	3.44 x 10 ¹¹

Areas occupied by hemipelagic clay, calcareous ooze, and siliceous ooze at the feather edge of stability for latitudes between 45° and 75°.

Cumulative methane flux (kg/m ²) for latitudes 45° - 75° and longitude -180° - 180°						
Sediment type	After 50 years	After 100 years	After 150 years	After 200 years	After 250 years	After 300 years
	4.24	23.50	31.15	34.07	35.64	36.65
Calcareous ooze	2.57	16.86	24.17	27.08	28.80	29.93
Siliceous ooze	3.19	37.40	50.58	52.08	52.88	53.41

The cumulative methane flux (kg/m²) from hemipelagic clay, calcareous ooze, and siliceous ooze at latitudes between 45° and 75° in 50-year intervals.

Cumulative mass of methane (kg) for latitudes 45° - 75° and longitude -180° - 180°						
Sediment type	After 50 years	After 100 years	After 150 years	After 200 years	After 250 years	After 300 years
Hemipelagic clay	3.48 x 10 ¹²	1.93 x 10 ¹³	2.56 x 10 ¹³	2.80 x 10 ¹³	2.93 x 10 ¹³	3.01 x 10 ¹³
Calcareous ooze	1.43 x 10 ¹¹	9.39 x 10 ¹¹	1.35 x 10 ¹²	1.51 x 10 ¹²	1.60 x 10 ¹²	1.67 x 10 ¹²
Siliceous ooze	1.10 x 10 ¹²	1.29 x 10 ¹³	1.74 x 10 ¹³	1.79 x 10 ¹³	1.82 x 10 ¹³	1.84 x 10 ¹³

The cumulative mass of methane (kg) from hemipelagic clay, calcareous ooze, and siliceous ooze at latitudes between 45° and 75° in 50-year intervals. This table is the product of the multiplication of the area occupied by each sediment and the cumulative methane flux for each sediment.